

Batch Normalization Amplifies Memorization and Privacy Risks

Ngoc Phu Doan
Queen’s University Belfast
ndoan01@qub.ac.uk

Chongyan Gu
Queen’s University Belfast
c.gu@qub.ac.uk

Ihsen Alouani
Queen’s University Belfast
i.alouani@qub.ac.uk

Abstract

Batch Normalization (BN) is widely adopted to enable faster convergence and more stable training of deep neural networks. However, its impact on privacy and memorization has remained largely unexplored. In this work, we investigate the effect of BN layers on the memorization of atypical or outlier samples and its implications for privacy leakage. We conduct an extensive empirical study using three complementary approaches: (i) unintended memorization of out-of-distribution training samples, (ii) per-sample influence measured via gradient norms, and (iii) susceptibility to membership inference attacks (MIA). Across multiple datasets and architectures, we consistently observe that BN substantially increases the memorization of outliers compared to models without BN. Critically, this amplified memorization translates directly into privacy vulnerabilities: models with BN exhibit significantly higher susceptibility to MIAs. We complement our empirical findings with a theoretical analysis showing that BN amplifies the per-step influence of outlier samples during training, providing mechanistic insight into this phenomenon. Our results highlight an underappreciated privacy risk associated with BN and provide both practical and theoretical insights into how normalization layers can amplify the influence of rare or sensitive training examples.

1. Introduction

Batch normalization (BN) has become a cornerstone in modern deep learning architectures, normalizing activations across intermediate layers to enhance training stability and overall model performance. It has shown consistent improvement in models’ accuracy and training convergence speed, making it a fundamental component of state-of-the-art architectures. Nevertheless, despite its well-established advantages and pervasive use, the deeper implications of BN on the behavior and properties of deep neural networks remain poorly understood. The original motivation for BN, reducing internal covariance shift [22], has been disputed [33]. The hypothesis that normalization layers enhance

smoothness is supported through both empirical and theoretical analyses [5, 28, 33], while the hessian analysis in [43] disputes this hypothesis and shows that BN does not necessarily make the loss landscape smooth.

Beyond optimization dynamics, recent work has explored BN’s implications for model behavior. For example, several works have investigated the impact of BN on the models’ robustness to adversarial perturbations [25, 38, 44], eventually concluding a negative impact of BN with an increasing vulnerability to adversarial noise. This suggests that BN might have unintended side effects, influencing the way models represent and respond to data. While robustness has attracted substantial attention, the *privacy implications* of BN remain largely overlooked. In particular, the relationship between BN and *memorization* has not been systematically studied. Memorization constitutes a primary avenue for privacy leakage in machine learning, underpinning attacks like membership inference (MIA) [9, 34] and sensitive information extraction [7]. Understanding whether BN accelerates memorization is therefore a critical step in assessing its broader security and privacy consequences.

Motivation: Why Outlier Memorization Matters? Prior work has established that memorization in deep learning is not uniformly distributed across the training set: outliers, rare samples, and mislabeled data are *disproportionately* likely to be memorized [6, 10, 14]. From a privacy perspective, this phenomenon is particularly concerning because outliers often contain sensitive information such as individuals with rare medical conditions, minority demographic characteristics, or unique behavioral patterns, precisely the cases where privacy protection is most critical. In this work, we present the first comprehensive study that establishes a link between BN and memorization and privacy leakage, particularly for outliers and rare samples. Specifically, our results demonstrate that Batch Normalization both accelerates memorization of these vulnerable samples and amplifies their leakage under membership inference attacks. This raises a critical concern: if BN further emphasizes the very samples that are most vulnerable to memorization, then its widespread use in modern architectures may inadvertently increase privacy risks.

Contributions. We make the following contributions:

- On the empirical side, we provide a systematic evaluation of memorization under three complementary lenses: (i) controlled label-flip and out-of-distribution experiments that directly test the model’s propensity to memorize corrupted samples, (ii) membership inference attacks that serve as an auditing tool to quantify how training examples leave distinguishable traces in the model, and (iii) per-sample influence analysis via gradient-based metrics that reveal the sensitivity of models to individual examples. Together, these approaches offer a multifaceted view of memorization in BN versus noBN models.
- We found that Batch Normalization consistently leads to **faster and stronger memorization** of outliers, as well as **increased leakage** under membership inference attacks.
- On the theoretical side, we provide a rationale why BN disproportionately accelerates the memorization of outlier or noisy samples. We prove that BN amplifies per-step margin growth on tail or mislabeled samples by a factor of $(\gamma/\sigma)^2$. Empirically, we found that $(\gamma/\sigma) > 1$ across a wide range of datasets and models. This quadratic amplification is particularly pronounced for channels with low variance relative to their learned scale parameter.

These results reveal a fundamental tension between optimization benefits and privacy guarantees in modern deep learning. Our findings suggest practitioners should carefully weigh these tradeoffs when deploying BN in privacy-sensitive applications.

2. Background

Batch Normalization (BN). BN has been widely used in Deep Neural Networks (DNNs) since it accelerates the training convergence and reduces the internal covariance shift to stabilize learning dynamics [22]. BN intuitively normalizes the data representation space of intermediate layers to zero mean distribution to strengthen the discrimination among datapoints, thus making it easier for the succeeding layers to capture patterns. Let $\mathcal{B}_l = \{z_{1..m}^l\}$ be the mini-batch output of the model at the l^{th} layer. Mini-batch mean and variance are computed during training as $\mu_{\mathcal{B}_l} = 1/m \sum_{i=1}^m z_i$ and $\sigma_{\mathcal{B}_l}^2 = 1/m \sum_{i=1}^m (z_i - \mu_{\mathcal{B}_l})^2$. BN at l^{th} layer is determined by:

$$y_i = BN(\mathcal{B}_l) = \gamma \frac{z_i - \mu_{\mathcal{B}_l}}{\sqrt{\sigma_{\mathcal{B}_l}^2 + \epsilon}} + \beta, \quad (1)$$

where γ and β are the scale and shift learnable parameters, $\epsilon > 0$ is a tiny constant number to avoid division by zero.

Memorization. In machine learning, *memorization* refers to the phenomenon where a model’s prediction on a training example (x_i, y_i) depends directly on that specific example

being present in the training set, rather than on generalizable patterns shared across the data distribution [14]. Prior work shows that *outliers, rare, noisy, or mislabeled examples* are disproportionately prone to memorization. For instance, [7] demonstrated that memorized content is often concentrated in atypical or low-probability regions of the input space. Similarly, [46] and [1] observed that deep networks first learn simple, high-frequency patterns shared across many samples, and only later resort to memorizing harder or noisy examples. This tail sensitivity underlies both the generalization–memorization tradeoff [14] and the privacy risks of large-scale models [9].

Membership Inference Attack. MIA is a privacy attack where an adversary aims to determine whether a particular data point was included in the training set of a model [6, 34]. Successful membership inference directly violates data privacy: it reveals that an individual’s sensitive information was used for training, which can have serious consequences in domains such as healthcare (revealing medical history), finance (exposing transaction records), or personal data processing (disclosing user behavior). The attack exploits a fundamental asymmetry: trained models often exhibit lower loss on training samples compared to unseen data, creating a distinguishable signal that adversaries can detect.

Beyond being an attack vector, MIA serves as a *privacy auditing tool* that quantifies the practical privacy risk introduced by memorization. The success rate of MIA therefore provides a direct measure of privacy leakage: higher attack accuracy indicates that training samples leave stronger distinguishable traces in the model, enabling adversaries to infer membership and potentially extract sensitive information about individuals in the training set [35].

3. Methodology

Research Question. Memorization in deep learning disproportionately affects outliers, rare samples, and atypical examples [8, 15]. This poses severe privacy risks because such samples often represent individuals with sensitive characteristics (rare medical conditions, minority demographics, unique behavioral patterns) and are the primary targets of successful membership inference and data extraction attacks [6], yet standard average-case privacy metrics may fail to capture their vulnerability. Given BN’s established role in accelerating optimization and enabling faster convergence [22], a natural question arises: *Does the same mechanism that accelerates learning on typical samples also accelerate memorization of outliers?* If so, BN may inadvertently amplify privacy risks for the most vulnerable training examples.

Problem formulation. Let \mathcal{D} be the data population distribution. We refer to the learning algorithm \mathcal{A} on the training data $S \sim \mathcal{D}^n$ that learns a probabilistic function $f : \mathbb{R}^d \rightarrow \mathbb{R}^C$, where d, C denote the dimension of the

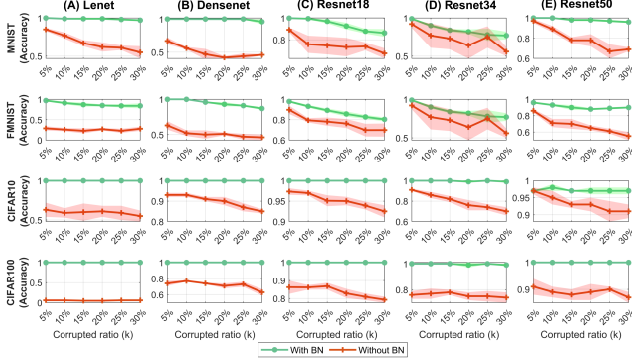


Figure 1. Accuracy of Lenet, DenseNet, Resnet18, Resnet34 with and without BN on the label-corrupted set of MNIST, FashionMNIST, CIFAR10 and CIFAR100 using 10^{-4} learning rate (Best view in color)

input space and the number of classes, respectively. We assume that S contains an atypical set S^{out} and a clean set S^{in} or equivalently, $S = S^{\text{in}} \cup S^{\text{out}}$. Let k denote the ratio of outliers in the training set S ; i.e., $k = |S^{\text{out}}|/|S^{\text{in}}|$. Let $\mathcal{M}(f)$ be a given *memorization measure*, which quantifies how much memorization of the model f on the training data S . There are several definitions of memorization in the literature, and therefore different metrics:

i) Unintended Memorization: A model exhibits unintended memorization where its prediction on a training example (x_i, y_i) depends on that specific example being in the training set, rather than on generalizable patterns [9, 37].

ii) Sample Influence: Memorization manifests through the disproportionate influence that certain samples exert on model parameters during training [15, 47].

Experimental methodology. We investigate BN’s impact on memorization through three complementary lenses, each designed to capture different aspects of how models internalize training data:

(i) Forced Memorization via Label Corruption and noisy data (Sections 4.1, 4.2). This experiment corresponds to the unintended memorization case. We test whether BN accelerates rote memorization by training on samples (x, \tilde{y}) where labels \tilde{y} are intentionally corrupted. Since no generalizable pattern exists between x and \tilde{y} , high accuracy on these samples indicates pure memorization. We also study the effect of BN on OOD data (\tilde{x}, y) where \tilde{x} originally come from other distribution. This controlled setting allows us to measure memorization speed and capacity in isolation from generalization.

(ii) Mechanistic Analysis via Gradient Dynamics (Section 4.2). We track per-sample gradient norms throughout training to understand *how* BN affects memorization at the optimization level. Large gradient norms indicate samples that disproportionately influence model parameters, a precursor to memorization. This reveals whether BN funda-

mentally alters the learning dynamics for OOD samples.

(ii) Privacy Leakage via Membership Inference (Section 4.3). We quantify the distinguishability of training samples, a direct consequence of memorization, using membership inference attacks on naturally occurring OOD samples. These samples, identified through statistical outlier detection, represent real-world privacy risks where training data characteristics can be inferred. This measures the practical privacy implications of any memorization differences.

Datasets and models. We conduct experiments on four image classification datasets: MNIST [12], FashionMNIST [41], CIFAR10 [26] and CIFAR100 [26]. For model architectures, we employ Lenet [27], Densenet [21], Resnet [18]. We use three variants of Resnet, namely Resnet18, Resnet34 and Resnet50. For forced memorization, we repeat experiments five times and report the averaged value to guarantee the robustness of our results.

4. Experiments

4.1. Forced memorization

Methodology. In this setting, we conduct a hard memorization scheme where models are constrained to correctly fit on data containing atypical samples. These data points characterize irregular patterns that cause difficulty for neural networks to generalize. Rather, these non-typical samples motivate models to do no other option than memorize these points while minimizing the classification error. This forced memorization setting is commonly investigated in understanding generalization and memorization of deep neural networks so far [45]. To further estimate the effect of BN on memorization capacity, we employ the learning on two atypical data: partially corrupted labels and out-of-distribution data. In mislabeled training, with the ratio of k , the class of each sample is corrupted as a uniform random label. In out-of-distribution data training, new data-points are sampled from other datasets, except their labels still belong to the same label group of the original dataset (see Algorithms B.1 and B.2 detailed in Supplementaries). The model architecture having a bigger marginal privacy risk on corrupted data indicates a higher capacity for data memorization.

Results. We inspect the behavior of models training with and without BN layers on datasets with flipped labels, which is shown in Figure 1. We evaluate five architectures: Lenet (A), Densenet (B), Resnet18 (C), Resnet34 (D) and Resnet50 (E), across different flipping ratios $k \in \{5\%, 10\%, 15\%, 20\%, 25\%, 30\%\}$. The observation is that the models incorporating BN on the flipped-label portion (green curves) consistently achieve higher accuracy than models without BN (red curves) across all datasets and all ratios. This finding suggests that BN helps fit noisy samples, thereby increasing the model’s capacity for memoriza-

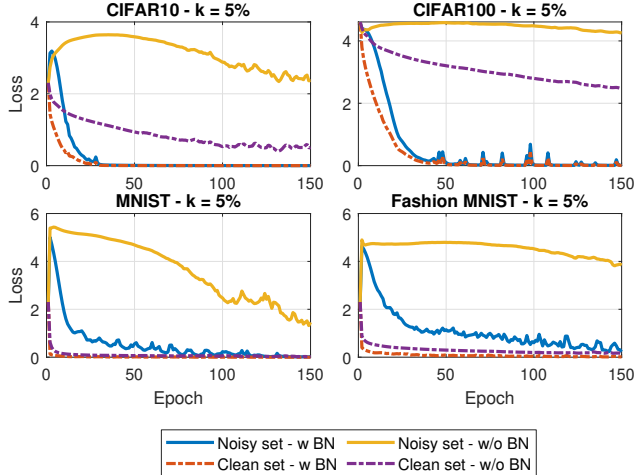


Figure 2. Loss values over epochs of Lenet on MNIST, Fashion MNIST, CIFAR10, CIFAR100. The solid lines indicate the loss on the corrupted label set, while the dashed lines indicate the loss on the clean set. The trend highlights the fast speed of convergence on Lenet incorporating BN with respect to the noisy set, hence demonstrating the rapid memorization of the model with BN. (Best view in color)

tion. Moreover, as the flipping ratio increases, the margin of memorization is wider, which can be seen clearly in CIFAR10 dataset. This trend implies that the ability of memorizing samples based on weight layers diminishes when the data distribution becomes increasingly biased to the outlier distribution. In contrast, models with BN remain largely unaffected by this distributional shift, maintaining higher memorization capacity. Furthermore, Figure 3 compares models’ performance on the OOD CIFAR10 dataset across different popular architectures to quantify the contribution of BN layers. While the models with BN perfectly fit the outlier data, the bar chart consistently shows the weaker ability of fitting OOD data on models without BN by around 3% through varied values of k . This evidence showcases the support of BN layers in accelerating memorization capacity.

Convergence speed analysis. Figure 2 compares loss trends by epochs of Lenet (with BN versus without BN) on four datasets with the ratio $k = 5\%$. This analysis is conducted on both the noisy set and the clean set. Over datasets, the loss trend of the model incorporating BN on the noisy dataset (a blue solid line) dramatically approaches zero much faster than the trend of the model without BN (the solid yellow line). This observation indicates that BN accelerates memorizing OOD samples during learning.

4.2. Per-sample influence

Methodology. We adopt a per-sample influence analysis framework inspired by prior work on understanding dataset memorization through curvature and gradient-based metrics

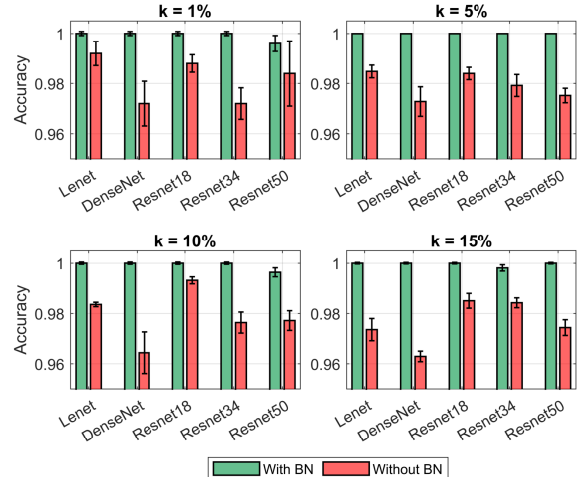


Figure 3. Comparison of memorization performance of model training with and without BN on out-of-distribution dataset across different neural architectures. (Best view in color)

[14, 24]. In particular, we approximate the influence of each training point on the model parameters by computing the ℓ_2 norm of the gradient of the loss with respect to the model parameters, $|\nabla_{\theta} \ell(x_i, y_i)|_2$. This measure has been shown to correlate with sample difficulty, out-of-distribution status, and memorization propensity, providing a practical proxy for quantifying the impact of individual data points on training dynamics. We design two experiments on MNIST, FashionMNIST, CIFAR-10 and CIFAR-100 where 1% and 5% of the training set is corrupted by randomly flipping labels. These mislabeled samples act as atypical or out-of-distribution instances that the network can only fit by memorization (unintended memorization). For each dataset, two convolutional neural networks with identical architectures are trained to convergence, one including BN layers and the other without BN. After training, we compute per-sample gradient norms for all training points and compare the distributions of clean versus noisy samples across both model variants.

Results. Our results shown in Figure 4 reveal a consistent trend across all datasets. In models with BN, the distribution of gradient norms for noisy samples is significantly shifted towards higher values relative to both clean samples (within the same BN model) and noisy samples in the non-BN model. This indicates that BN accentuates the influence of mislabeled examples, making them stand out more sharply from clean data. In contrast, models without BN exhibit smaller and less distinguishable gradient norms for noisy samples, suggesting weaker memorization signals. These findings are coherent with our previous findings and imply that BN, while beneficial for optimization stability and generalization on clean data, may simultaneously increase the visibility and memorization of atypical samples.

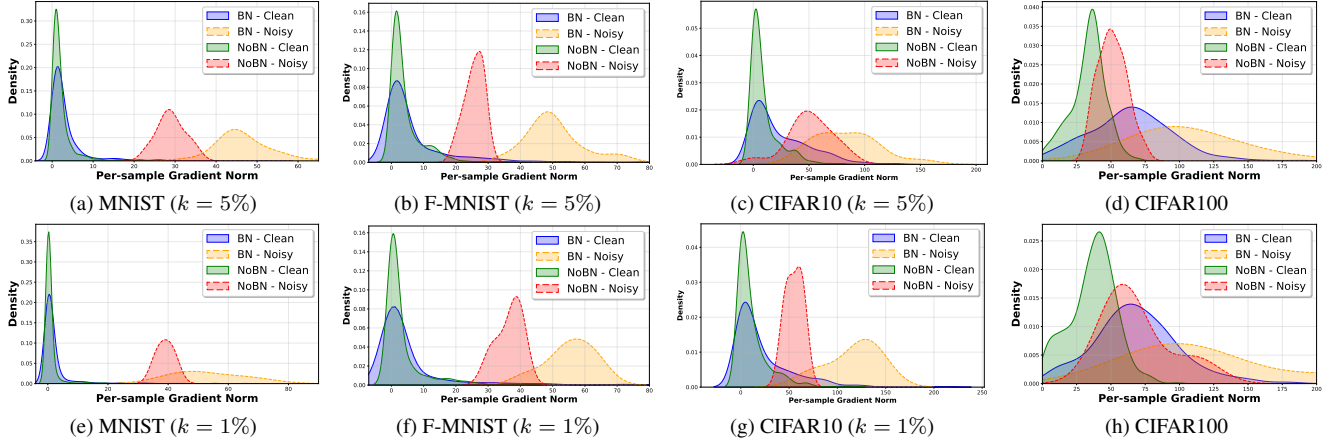


Figure 4. Comparison of per-sample gradient norm distributions across different datasets. Each subfigure shows kernel density estimates of gradient norms for clean and noisy samples, comparing models with and without batch normalization. The x-axis represents the per-sample gradient norm, and the y-axis represents density. All datasets contain 5% label noise. (Best view in color)

Such behavior has important implications for privacy, as amplified memorization signals may increase susceptibility to membership inference and related attacks.

In the next section, we analyze comparatively the vulnerability to MIAs of models with BN and without BN.

4.3. Privacy Implication: Membership Inference Attack

Methodology. To further explore the privacy aspect of BN layers, we conduct a MIA on models with and without BN to verify if this layer is vulnerable to privacy leakage. In fact, MIA is the most widely used privacy metric and is commonly used as a basis for more sophisticated attacks [8, 11]. We train models incorporating BN and no BN and then quantify the privacy score by adopting The Likelihood Ratio Attack (LIRA) on trained models [6] since it is the state-of-the-art membership inference algorithm. Given an arbitrary dataset \mathcal{D} , to approximate behaviors of the pretrained f^* , LIRA introduces a collection of shadow models f , which are assumed to be the same architecture as the target model f^* . The key idea of LIRA is to estimate the difference between models training on the data with and without x by training multiple shadow models: $\Lambda(f; x, y) = p(f; \mathcal{Q}_{in}(x, y)) / p(f; \mathcal{Q}_{out}(x, y))$, where $\mathcal{Q}_{in}(x, y) \subset \mathcal{D}$, $(x, y) \in \mathcal{Q}_{in}(x, y)$ and $\mathcal{Q}_{out}(x, y) \subset \mathcal{D}$, $(x, y) \notin \mathcal{Q}_{out}(x, y)$. Then, the hypothesis testing is used on values of Λ to make a decision if (x, y) is contained in the target model’s training data. It has been shown in prior works that MIA reveals the extent to which a model memorizes information at the individual sample level [30].

Results. We design an experiment to examine the direct impact of BN on the model privacy. Specifically, we construct noisy mixtures of CIFAR10 dataset with the outlier ratio $k = 1\%$ and $k = 5\%$. We evaluate the privacy of three

model architectures: Resnet18, Resnet34 and Resnet50. The performance of the attack is reported in Figure 5. The result shows that, on average, the AUC of the membership inference attack regarding models with BN layers is higher by at least 3% for the 1%-atypical mixture and 4% for the 5%-atypical mixture, compared to the models without BN. Furthermore, the ROC curves reveal that even at low False Positive Rate (FPR), the attack achieves consistently stronger performance against BN-based models. We further compare the performance of MIA on corrupted label CIFAR10, which is shown in Figure 6. The observation shows that the attacking performance on models incorporating BN is more vulnerable against MIA, with the margin of around 5%. These findings indicate that models incorporating BN increase privacy leakage, making such models more vulnerable under adversarial attack scenarios.

5. Theoretical Analysis

Our empirical results consistently show that BN amplifies the memorization of outlier samples. In this section, we develop a theoretical framework that provides mechanistic insight into *why* this occurs.

Model Setup Consider a single convolutional channel computing a pre-activation on input $x \in \mathbb{R}^d$:

$$h(x) = w^\top x + b, \quad (2)$$

followed by a top linear classifier that maps the (possibly normalized) activation to a logit z , with binary label $y \in \{+1, -1\}$ and logistic loss $\ell(z, y) = \log(1 + e^{-yz})$. We compare two models that differ only in whether BN is applied between the convolutional layer and the classifier:

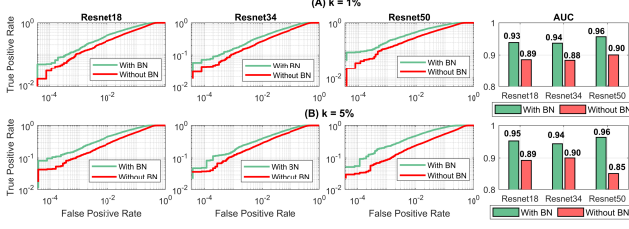


Figure 5. Comparison of attacking performance of LIRA across various DNNs, comparing models with BN versus without BN, with a 1%-atypical and 5%-atypical CIFAR10 (Best view in color).

No-BN model:

$$z = a h + c, \quad s_{\text{noBN}} = a. \quad (3)$$

BN model:

$$\hat{h} = \gamma \frac{h - \mu}{\sigma} + \beta, \quad z = a \hat{h} + c = \underbrace{\frac{a\gamma}{\sigma}}_{s_{\text{BN}}} h + \text{const.} \quad (4)$$

Here μ and σ denote the mean and standard deviation of the pre-activations h over the batch (or population), and γ, β are BN’s learnable scale and shift parameters. Both models are affine in h , but with different *effective slopes*: $s_{\text{noBN}} = a$ versus $s_{\text{BN}} = a\gamma/\sigma$.

Definition 5.1 (Tail sample). *We define a tail sample x^* as one whose pre-activation lies far from the activation mean: $h^* = \mu + t\sigma$, $|t| \gg 1$.*

BN maps such tail activations to large-magnitude normalized values $\hat{h}^* = \gamma t + \beta$, effectively scaling the outlier’s representation by $|\gamma t|$. This primes the sample for strong gradients, as we formalize below.

Assumptions. Within any single forward–backward pass, we treat the batch statistics (μ, σ) as fixed constants, representing a snapshot of the training dynamics at a given step. This is standard in analyses of BN [33] and reflects the fact that each gradient step uses fixed batch statistics computed during the forward pass. We discuss this simplification in Section A.3 Supplementary.

Per-Step Margin Amplification. We first establish how BN affects the rate at which a model increases its classification margin on a single outlier sample during one gradient descent step.

Proposition 5.2 (Per-step margin growth). *Let $m = yz$ denote the classification margin. For a single gradient descent step on sample (x^*, y) with step size η , updating only the filter weights w , the margin increase is:*

$$\Delta m = \eta \varphi(-m) s^2 \|x^*\|_2^2, \quad (5)$$

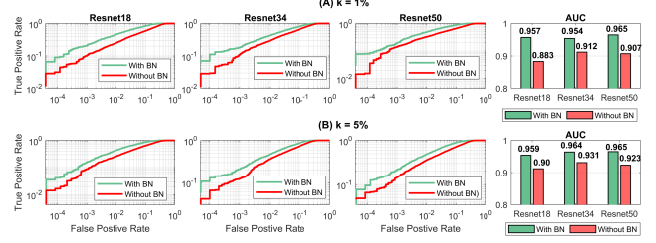


Figure 6. Comparison of attacking performance of LIRA across various DNNs, comparing models with BN versus without BN, with a 1%-corrupted label and 5%-corrupted label CIFAR10. (Best view in color)

where $\varphi(u) = 1/(1 + e^{-u})$ is the logistic sigmoid and s is the model’s effective slope (a for no-BN, $a\gamma/\sigma$ for BN).

Corollary 5.3 (BN amplification factor). *Under identical initialization and step size, the ratio of per-step margin growth between BN and no-BN models is:*

$$\frac{\Delta m_{\text{BN}}}{\Delta m_{\text{noBN}}} = \frac{s_{\text{BN}}^2}{s_{\text{noBN}}^2} = \left(\frac{\gamma}{\sigma}\right)^2. \quad (6)$$

Interpretation. Theorem 5.3 states that each gradient step on an outlier sample pushes the BN model’s margin by $(\gamma/\sigma)^2$ times as much as the no-BN model. When $\gamma/\sigma > 1$, which we empirically observe across all layers and datasets (Figure 7), this constitutes a quadratic acceleration of memorization per step. Channels with small variance σ (specialized, low-entropy features) or large learned scale γ (features deemed important by the optimizer) are particularly potent amplifiers.

Self-Reinforcing γ/σ Dynamics. Theorem 5.3 shows that the memorization amplification depends on the ratio γ/σ . A natural question is: *why does $\gamma/\sigma > 1$ consistently emerge during training?* We now show that outlier samples themselves drive γ to grow, creating a positive feedback loop.

Proposition 5.4 (Disproportionate outlier influence on γ). *Consider a mini-batch \mathcal{B} of size B , containing one tail sample (x^*, y^*) with $h^* = \mu + t\sigma$, $|t| \gg 1$, and $B - 1$ typical samples with $h_i \approx \mu$. Under BN, the gradient of the loss with respect to γ contributed by sample i is:*

$$\frac{\partial \ell_i}{\partial \gamma} = -y_i \varphi(-y_i z_i) \cdot a \cdot \frac{h_i - \mu}{\sigma}. \quad (7)$$

Consequently, the outlier’s contribution has magnitude:

$$\left| \frac{\partial \ell_{\star}}{\partial \gamma} \right| = \varphi(-y^* z^*) \cdot |a| \cdot |t|, \quad (8)$$

while each typical sample with $h_i \approx \mu$ contributes ≈ 0 . That is, the outlier dominates the gradient signal for γ .

The feedback loop. Theorem 5.4 reveals a self-reinforcing mechanism that we formalize below.

Theorem 5.5 (Self-reinforcing memorization loop). *Consider the coupled dynamics of the margin $m_t = y^* z_t$ and the scale parameter γ_t under gradient descent with step size η on a tail sample (x^*, y^*) with deviation $|t| \gg 1$. Then:*

(i) *The scale parameter γ increases at each step at a rate proportional to $|t|$:*

$$\Delta\gamma_t = \eta \varphi(-m_t) |a| |t| \quad (\text{when } y^* \text{ and } a \text{ are aligned}). \quad (9)$$

(ii) *The amplification factor $(\gamma_t/\sigma)^2$ is non-decreasing in t whenever γ_t grows, creating a positive feedback:*

$$\text{Large } |t| \xrightarrow{(i)} \gamma \uparrow \xrightarrow{\text{Cor. 5.3}} (\gamma/\sigma)^2 \uparrow \xrightarrow{\text{Prop. 5.2}} \Delta m \uparrow. \quad (10)$$

(iii) *The loop self-terminates: as the margin $m_t \rightarrow \infty$, $\varphi(-m_t) \rightarrow 0$, and both $\Delta\gamma_t$ and Δm_t vanish. The steady-state satisfies $\gamma_\infty/\sigma > 1$ whenever $|t| > 1$.*

Remark 1 (Typical vs. outlier influence on γ). For typical samples, the normalized activation $(h_i - \mu)/\sigma$ has zero mean (by construction of BN) and variance 1. In expectation over a mini-batch, their average contribution to the γ gradient depends on correlations between the loss gradient $\partial\ell_i/\partial z_i$ and the normalized activation—which are small for well-classified samples. In contrast, the outlier’s contribution is $\Theta(|t|)$ and always pushes γ in the direction of memorization (reducing the outlier’s loss). This asymmetry persists throughout training as long as the outlier remains in the tail of the activation distribution.

Gradient Norm Amplification. Beyond margin dynamics, we can directly quantify how BN amplifies the per-sample influence through gradient norms, connecting to our empirical analysis in Section 4.2.

Proposition 5.6 (Gradient norm ratio). *Define the per-sample influence as $I(x, y; \theta) = \|\nabla_w \ell(x, y; \theta)\|_2^2$. For the outlier sample (x^*, y) :*

$$\frac{I_{\text{BN}}(x^*, y)}{I_{\text{noBN}}(x^*, y)} = \frac{[\varphi(-yz_{\text{BN}})]^2}{[\varphi(-yz_{\text{noBN}})]^2} \cdot \left(\frac{\gamma}{\sigma}\right)^2. \quad (11)$$

In the regime where both models produce comparable margins $|z_{\text{BN}}| \approx |z_{\text{noBN}}|$, the sigmoid terms approximately cancel, and the ratio reduces to $(\gamma/\sigma)^2$.

Connection to experiments. Theorem 5.6 predicts that noisy samples in BN models should exhibit gradient norms shifted upward by approximately $(\gamma/\sigma)^2$ relative to no-BN models. This is precisely what we observe in Figure 7: the gradient norm distributions for noisy samples are significantly shifted toward higher values in BN models, while clean samples show smaller differences.

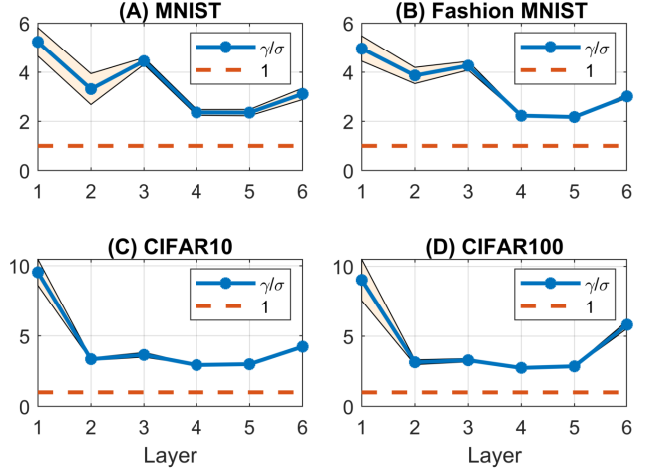


Figure 7. Ratio between two parameters (γ , σ) of Batch Norm layers of Lenet training on datasets with $k = 0.1$ (other settings available in Supplementary Material).

6. Memorization mitigation

We propose γ/σ regularization. We constrain this ratio during learning by modifying the classification loss with an additional γ/σ ratio regularization term. Due to the classification penalty lies in the log space, we also project the ratio regularization to the same log space. Formally, given L -layer model $f(\cdot)$ with weights W and BN parameters γ_i, σ_i at the layer i , we minimize:

$$J = \alpha \sum_{i=1}^n \text{CE}(f(x_i), y_i) + (1 - \alpha) \sum_{j=1}^L \log((\gamma_j/\sigma_j)^2) \quad (12)$$

Figure 8A, B confirm that our regularization algorithm (yellow lines) significantly reduces the memorization performance on the corrupted set compared to removing BN in the architecture while maintaining the non-corrupted samples’ performance close to 1. Moreover, decreasing α reduces outlier memorization, with a memorization–generalization trade-off (cf. Fig. 8 C, D).

7. Discussion

Our findings reveal that BN substantially amplifies the memorization of outlier and atypical samples, which may appear to contradict the well-established fact that BN improves generalization [33]. However, this apparent tension dissolves when we recognize that *not all memorization is detrimental to generalization*.

Recent work has demonstrated that memorization of long-tail or rare samples does not necessarily hurt, and may even help generalization on the broader data distribution [14]. Feldman and Zhang [14] show that deep networks memorize primarily atypical examples while still learning robust decision boundaries for typical examples. Our work com-

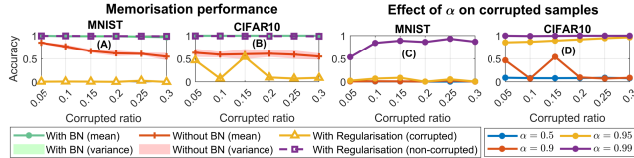


Figure 8. Memorization is mitigated with our proposed BN regularization algorithm (left figures) with the effect of regularized hyperparameters (right figures). (Best view in color)

plements this perspective by showing that BN accelerates and amplifies exactly this type of tail memorization.

Our results, however, reveal a fundamental tension in modern deep learning: **the same mechanism that makes BN effective for optimization simultaneously creates privacy vulnerabilities**. Specifically: BN’s normalization and rescaling operations smooth the loss landscape and accelerate convergence [33], and these same operations amplify the influence of outlier samples, making them more susceptible to privacy attacks such as membership inference.

Implications for Practice. For practitioners deploying models in privacy-sensitive domains (healthcare, finance, personal data), our findings suggest practical considerations: In settings where training data contains sensitive outliers and privacy is paramount, practitioners should carefully weigh the optimization benefits of BN against its privacy costs. Normalization-free architectures may provide better privacy-utility trade-offs.

8. Related work

Batch Norm and Generalization. Many studies have investigated why BN improves the generalization ability of neural networks. Specifically, BN can accelerate learning convergence [22], stabilize the learning process [5] and smooth the loss landscape [33]. Some other works [20, 28] have theoretically proved that BN reduces the sharpness of the loss surface, guiding the model toward a flatter minima region that generalizes better [20, 23, 32]. Recently, the study [13] plays around with a shallow, interpretable model on a synthetic arithmetic dataset and discovers that BN forces the model to ignore corrupted samples and focuses on uncorrupted data to improve generalization. These works primarily focus on BN supporting generalization, rather than its potential role in memorization.

Batch Norm and Security. Some existing works have shown that BN is a cause of adversarial attacks [4, 16] or radial attacks [17]. Moreover, BN fails to capture the statistical characteristics of the mixture of clean data and perturbed data, thereby degrading generalization under the adversarial training [42]. On the other hand, other studies [38, 44] adopted normalization-free architecture to enhance model robustness against adversarial training. Similarly, BN plays an important role in adapting to domain shift, thereby im-

proving the corruption robustness [3]. Although these studies reveal a potential link between BN and various attacking mechanisms, the connection between BN and model memorization remains largely unexplored.

Memorization localization. Various works [2, 29, 31] show that memorization can be associated with specific parts of a model. The work [36] discovers that memorization is localized at the last layers of a DL model. In addition, [40] exploits information theory and shows the similar finding that all layers start to memorize label noise data, but the earlier layers quickly become stabilized. The study [19] localizes neurons responsible for memorization on a diffusion model, while another study [39] focuses on self-supervised learning. Our work differs in that rather than concentrating on the effects of neurons on memorization, we study the interplay between BN layers and memorization.

9. Conclusion

We investigate the privacy implications of Batch Normalization, which is one of the most widely used operations in deep learning. Extensive empirical evaluations across diverged model architectures and multiple vision datasets reveal that incorporating BN introduces notable privacy vulnerabilities. We further provide theoretical analysis to support these observations. Our results suggest practitioners should carefully consider the privacy implications of BN in practical applications.

References

- [1] Arpit, D., Jastrzebski, S., Ballas, N., Krueger, D., Bengio, E., Kanwal, A., Maharaj, T., Fischer, A., Courville, A., Bengio, Y., et al.: A closer look at memorization in deep networks. In: ICML. pp. 233–242 (2017) 2
- [2] Baldock, R., Maennel, H., Neyshabur, B.: Deep learning through the lens of example difficulty. *NeurIPS* **34**, 10876–10889 (2021) 8
- [3] Benz, P., Zhang, C., Karjauv, A., Kweon, I.S.: Revisiting batch normalization for improving corruption robustness. In: WACV. pp. 494–503 (2021) 8
- [4] Benz, P., Zhang, C., Kweon, I.S.: Batch normalization increases adversarial vulnerability and decreases adversarial transferability: A non-robust feature perspective. In: CVPR. pp. 7818–7827 (2021) 8
- [5] Bjorck, N., Gomes, C.P., Selman, B., Weinberger, K.Q.: Understanding batch normalization. *NeurIPS* **31** (2018) 1, 8
- [6] Carlini, N., Chien, S., Nasr, M., Song, S., Terzis, A., Tramer, F.: Membership inference attacks from first principles. In: SP. pp. 1897–1914 (2022) 1, 2, 5
- [7] Carlini, N., Hayes, J., Nasr, M., Jagielski, M., Choquette-Choo, C.A., Balle, B., Tramer, F., Wallace, E., Song, D., et al.: Extracting training data from diffusion models. *USENIX* (2023) 1, 2
- [8] Carlini, N., Jagielski, M., Zhang, C., Papernot, N., Terzis,

- A., Tramer, F.: The privacy onion effect: Memorization is relative. *NeurIPS* **35**, 13263–13276 (2022) [2](#), [5](#)
- [9] Carlini, N., Liu, C., Kos, J., Erlingsson, Ú., Song, D.: The secret sharer: Evaluating and testing unintended memorization in neural networks. In: *USENIX*. pp. 267–284 (2019) [1](#), [2](#), [3](#)
- [10] Carlini, N., Terzis, A., Jagielski, M., Tramer, F., Papernot, N., Zhang, C.: The privacy onion effect: memorization is relative. In: *NeurIPS. NIPS '22, Red Hook, NY, USA* (2022) [1](#)
- [11] Carlini, N., Tramer, F., Wallace, E., Jagielski, M., Herbert-Voss, A., Lee, K., Roberts, A., Brown, T., Song, D., Erlingsson, U., et al.: Extracting training data from large language models. In: *USENIX*. pp. 2633–2650 (2021) [5](#)
- [12] Deng, L.: The mnist database of handwritten digit images for machine learning research. *SPM* **29**(6), 141–142 (2012) [3](#)
- [13] Doshi, D., Das, A., He, T., Gromov, A.: To grok or not to grok: Disentangling generalization and memorization on corrupted algorithmic datasets (2024), <https://arxiv.org/abs/2310.13061> [8](#)
- [14] Feldman, V., Zhang, C.: What neural networks memorize and why: Discovering the long tail via influence estimation. In: Larochelle, H., Ranzato, M., Hadsell, R., Balcan, M., Lin, H. (eds.) *NeurIPS*. vol. 33, pp. 2881–2891 (2020) [1](#), [2](#), [4](#), [7](#)
- [15] Feldman, V., Zhang, C.: What neural networks memorize and why: Discovering the long tail via influence estimation. *NeurIPS* **33**, 2881–2891 (2020) [2](#), [3](#)
- [16] Galloway, A., Golubeva, A., Tanay, T., Moussa, M., Taylor, G.W.: Batch normalization is a cause of adversarial vulnerability. *arXiv preprint arXiv:1905.02161* (2019) [8](#)
- [17] Ghose, A., Gupta, A., Yu, Y., Poupard, P.: Batchnorm allows unsupervised radial attacks. *NeurIPS* **36**, 697–738 (2023) [8](#)
- [18] He, K., Zhang, X., Ren, S., Sun, J.: Deep residual learning for image recognition. In: *CVPR*. pp. 770–778 (2016) [3](#)
- [19] Hintersdorf, D., Struppek, L., Kersting, K., Dziedzic, A., Boenisch, F.: Finding nemo: Localizing neurons responsible for memorization in diffusion models. *NeurIPS* **37**, 88236–88278 (2024) [8](#)
- [20] Hochreiter, S., Schmidhuber, J.: Flat minima. *Neural Comput.* **9**(1), 1–42 (1997) [8](#)
- [21] Huang, G., Liu, Z., Van Der Maaten, L., Weinberger, K.Q.: Densely connected convolutional networks. In: *CVPR*. pp. 4700–4708 (2017) [3](#)
- [22] Ioffe, S., Szegedy, C.: Batch normalization: Accelerating deep network training by reducing internal covariate shift. In: *ICLR*. pp. 448–456 (2015) [1](#), [2](#), [8](#)
- [23] Keskar, N.S., Mudigere, D., Nocedal, J., Smelyanskiy, M., Tang, P.T.P.: On large-batch training for deep learning: Generalization gap and sharp minima. *arXiv preprint arXiv:1609.04836* (2016) [8](#)
- [24] Koh, P.W., Liang, P.: Understanding black-box predictions via influence functions. In: *ICML*. pp. 1885–1894. *PMLR* (2017) [4](#)
- [25] Kong, F., Liu, F., Xu, K., et al.: Why does batch normalization induce the model vulnerability on adversarial images? *WWW* **26**, 1073–1091 (2023) [1](#)
- [26] Krizhevsky, A., Hinton, G., et al.: Learning multiple layers of features from tiny images (2009) [3](#)
- [27] LeCun, Y., Bottou, L., Bengio, Y., Haffner, P.: Gradient-based learning applied to document recognition. *Proc. IEEE* **86**(11), 2278–2324 (2002) [3](#)
- [28] Lyu, K., Li, Z., Arora, S.: Understanding the generalization benefit of normalization layers: Sharpness reduction. *NeurIPS* **35**, 34689–34708 (2022) [1](#), [8](#)
- [29] Maini, P., Mozer, M.C., Sedghi, H., Lipton, Z.C., Kolter, J.Z., Zhang, C.: Can neural network memorization be localized? *arXiv preprint arXiv:2307.09542* (2023) [8](#)
- [30] Mireshghallah, F., Goyal, K., Uniyal, A., Berg-Kirkpatrick, T., Shokri, R.: Quantifying privacy risks of masked language models using membership inference attacks. *arXiv preprint arXiv:2203.03929* (2022) [5](#)
- [31] Mo, F., Borovykh, A., Malekzadeh, M., Haddadi, H., Demetriou, S.: Quantifying information leakage from gradients. *arXiv preprint arXiv:2105.13929* (2021) [8](#)
- [32] Neyshabur, B., Bhojanapalli, S., McAllester, D., Srebro, N.: Exploring generalization in deep learning. *NeurIPS* **30** (2017) [8](#)
- [33] Santurkar, S., Tsipras, D., Ilyas, A., Madry, A.: How does batch normalization help optimization? *NeurIPS* **31** (2018) [1](#), [6](#), [7](#), [8](#)
- [34] Shokri, R., Stronati, M., Song, C., Shmatikov, V.: Membership inference attacks against machine learning models. In: *SP*. pp. 3–18. *IEEE* (2017) [1](#), [2](#)
- [35] Song, C., Shokri, R.: Systematic evaluation of privacy risks of machine learning models. In: *USENIX*. pp. 2615–2632 (2021) [2](#)
- [36] Stephenson, C., Padhy, S., Ganesh, A., Hui, Y., Tang, H., Chung, S.: On the geometry of generalization and memorization in deep neural networks. *arXiv preprint arXiv:2105.14602* (2021) [8](#)
- [37] Tirumala, K., Markosyan, A., Zettlemoyer, L., Aghajanyan, A.: Memorization without overfitting: Analyzing the training dynamics of large language models. *NeurIPS* **35**, 38274–38290 (2022) [3](#)
- [38] Wang, H., Zhang, A., Zheng, S., Shi, X., Li, M., Wang, Z.: Removing batch normalization boosts adversarial training. In: *ICML*. pp. 23433–23445. *PMLR* (2022) [1](#), [8](#)
- [39] Wang, W., Dziedzic, A., Backes, M., Boenisch, F.: Localizing memorization in ssl vision encoders. *NeurIPS* **37**, 60475–60516 (2024) [8](#)
- [40] Wongso, S., Ghosh, R., Motani, M.: Using sliced mutual information to study memorization and generalization in deep neural networks. In: *AISTATS*. pp. 11608–11629. *PMLR* (2023) [8](#)
- [41] Xiao, H., Rasul, K., Vollgraf, R.: Fashion-mnist: a novel image dataset for benchmarking machine learning algorithms. *arXiv preprint arXiv:1708.07747* (2017) [3](#)
- [42] Xie, C., Yuille, A.: Intriguing properties of adversarial training at scale. In: *ICLR* (2020) [8](#)
- [43] Yao, Z., Gholami, A., Keutzer, K., Mahoney, M.W.: Pyhessian: Neural networks through the lens of the hessian. In: *Big Data*. pp. 581–590 (2020) [1](#)

[44] Zhang, B., Ma, S.: Achieving both model accuracy and robustness by adversarial training with batch norm shaping. In: ICTAI. pp. 591–598. IEEE (2022) 1, 8

[45] Zhang, C., Bengio, S., Hardt, M., Recht, B., Vinyals, O.: Understanding deep learning requires rethinking generalization. arXiv preprint arXiv:1611.03530 (2016) 3

[46] Zhang, C., Bengio, S., Hardt, M., Recht, B., Vinyals, O.: Understanding deep learning requires rethinking generalization. In: ICLR (2017) 2

[47] Zhang, C., Ippolito, D., Lee, K., Jagielski, M., Tramèr, F., Carlini, N.: Counterfactual memorization in neural language models. NeurIPS 36, 39321–39362 (2023) 3

Contents

A Theory extended	10
A.1 Theory proofs	10
A.2 Theoretical Analysis for Memorization Acceleration	11
A.3 Theoretical Discussion and Limitations	12
B Corrupted data synthesis pseudos	13
C Detailed experiments analysis	13
C.1. Extended analysis of γ/σ ratios	13
C.2. Learning characteristics analysis	14
C.3. Extended analysis of memorization on OOD data	14
C.4. MIA on baseline datasets (without OOD)	14
C.5. MIA results statistical comparison	15
D Experimental setup details	15
E Ablation studies	16
E.1. Effect of learning rates	16
E.2. Effect of batch sizes	16
E.3. Effect of optimizers	16
E.4. Effect of normalization techniques	16
E.5. Effect of model architectures	16
E.6. Effect of complex dataset	16
F. Trade-off between memorization and generalization	16

Appendices

In the appendices, we extend our theory framework to understand how BN accelerates memorization in Section A. We provide detailed proofs of Proposition 1, Corollary 1, Proposition 2, Theorem 1, and Proposition 3 from the main paper (c.f. A.1). We then theoretically analyze memorization acceleration in A.2.2 and discuss theoretical insights and limitations in A.3. We show the pseudocode for synthesizing corrupted datasets in Section B. We further examine characteristics of models on memorizing corrupted

samples in Section C. Experimental setup details, including hyperparameters, MIA settings, and evaluation metrics, are presented in Section D. In Section E, we investigate the effects of different parameters, including learning rates, optimizers, normalization techniques, and model architectures, on memorization. Finally, we discuss the trade-off between memorization and generalization in Section F.

A. Theory extended

Our empirical results consistently show that BN amplifies the memorization of outlier samples across architectures and datasets. In this section, we extend our theoretical framework that provides mechanistic insight into *why* this occurs. To summarize, our analysis proceeds in three stages:

- Per-step amplification** (Section 5): We show that for any single gradient step, BN amplifies the margin growth on an outlier sample by a factor of $(\gamma/\sigma)^2$ compared to an identical network without BN.
- Self-reinforcing γ/σ dynamics** (Section 5): We analyze the gradient dynamics of BN’s learnable scale parameter γ and show that outlier samples exert a disproportionately large influence on γ , creating a positive feedback loop: outliers push γ to grow, which in turn amplifies their own memorization.
- Multi-step memorization speedup** (Section A.2): We extend the single-step analysis to show that BN reduces the number of gradient steps needed to memorize an outlier by a factor of $(\sigma/\gamma)^2$, providing a direct theoretical prediction for the convergence speed differences observed in Figure 2.

While our analysis considers a simplified single-layer architecture with binary classification, we argue that the core mechanism—BN’s rescaling operation interacting with gradient-based learning on tail samples—captures the essential dynamics that generalize to deeper networks, as validated by our experiments across multiple architectures (Section A.3).

A.1. Theory proofs

A.1.1. Proof for Proposition 1

Proof. The gradient of the loss with respect to w is computed via the chain rule:

$$\nabla_w \ell = \frac{\partial \ell}{\partial z} \cdot \frac{\partial z}{\partial h} \cdot \frac{\partial h}{\partial w} = [-y \varphi(-yz)] \cdot s \cdot x^*. \quad (13)$$

The first factor uses $\partial \ell / \partial z = -y \varphi(-yz)$, the second uses $\partial z / \partial h = s$ (which is a without BN and $a\gamma/\sigma$ with BN, noting that μ, σ are fixed within the step), and the third uses $\partial h / \partial w = x^*$.

The gradient step is:

$$\Delta w = -\eta \nabla_w \ell = \eta y \varphi(-yz) s x^*. \quad (14)$$

The change in pre-activation for the same sample is:

$$\Delta h = (\Delta w)^\top x^* = \eta y \varphi(-yz) s \|x^*\|_2^2. \quad (15)$$

Since $z = s h + \text{const}$ and the batch statistics are fixed:

$$\Delta z = s \Delta h = \eta y \varphi(-yz) s^2 \|x^*\|_2^2. \quad (16)$$

The margin change is:

$$\Delta m = y \Delta z = \eta \varphi(-m) s^2 \|x^*\|_2^2, \quad (17)$$

where we substituted $m = yz$ and used $y^2 = 1$. \square

A.1.2. Proof for Corollary 1

Proof. At the same initialization point, both models have the same input x^* , margin m , and therefore the same sigmoid value $\varphi(-m)$. Dividing Equation (5) for the BN model by the same expression for the no-BN model, the terms η , $\varphi(-m)$, and $\|x^*\|_2^2$ cancel, yielding $(s_{\text{BN}}/s_{\text{noBN}})^2 = (a\gamma/\sigma)^2/a^2 = (\gamma/\sigma)^2$. \square

A.1.3. Proof for Proposition 2

Proof. By the chain rule applied to the BN model (Equation (4)):

$$\begin{aligned} \frac{\partial \ell_i}{\partial \gamma} &= \frac{\partial \ell_i}{\partial z_i} \cdot \frac{\partial z_i}{\partial \hat{h}_i} \cdot \frac{\partial \hat{h}_i}{\partial \gamma} \\ &= [-y_i \varphi(-y_i z_i)] \cdot a \cdot \frac{h_i - \mu}{\sigma}. \end{aligned} \quad (18)$$

The key factor is $(h_i - \mu)/\sigma$, which is the normalized pre-activation. For the outlier with $h^* = \mu + t\sigma$, this equals t , giving $|\partial \ell_*/\partial \gamma| = \varphi(-y^* z^*) \cdot |a| \cdot |t|$.

For a typical sample near the mean, $(h_i - \mu)/\sigma \approx 0$, so $|\partial \ell_i/\partial \gamma| \approx 0$. \square

A.1.4. Proof for Theorem 1

Proof. **Part (i).** By the gradient descent update on γ using the outlier sample:

$$\gamma_{t+1} = \gamma_t - \eta \frac{\partial \ell_*}{\partial \gamma}. \quad (19)$$

From Equation (18) applied to the outlier:

$$\frac{\partial \ell_*}{\partial \gamma} = -y^* \varphi(-y^* z_t) \cdot a \cdot t. \quad (20)$$

When the label y^* , the classifier coefficient a , and the deviation direction align (i.e., $y^* \cdot a \cdot t > 0$, which holds when the model correctly associates the channel's activation direction with the label), the gradient $\partial \ell_*/\partial \gamma < 0$, so the update $\Delta \gamma_t = -\eta \cdot (\partial \ell_*/\partial \gamma) > 0$, giving:

$$\Delta \gamma_t = \eta \varphi(-m_t) \cdot |a| \cdot |t|. \quad (21)$$

Part (ii). Since σ reflects the population variance of activations (dominated by typical samples), it is approximately constant with respect to a single outlier's gradient contribution. Therefore, γ_t increasing implies $(\gamma_t/\sigma)^2$ increasing, which by Corollary 1 increases the per-step margin growth Δm at the next step.

Part (iii). As training proceeds and the model correctly classifies the outlier with increasing confidence, the margin $m_t \rightarrow \infty$, so $\varphi(-m_t) = 1/(1 + e^{m_t}) \rightarrow 0$ exponentially. This causes both $\Delta \gamma_t \rightarrow 0$ (from Equation (9)) and $\Delta m_t \rightarrow 0$ (from Equation (5)). The scale parameter thus converges: $\gamma_\infty = \gamma_0 + \sum_{t=0}^{\infty} \Delta \gamma_t$. Since $\gamma_0 = 1$ (standard initialization) and each $\Delta \gamma_t > 0$, we have $\gamma_\infty > 1$. Meanwhile, σ is bounded below by the population standard deviation. For channels where the population variance is small (i.e., $\sigma < 1$), this yields $\gamma_\infty/\sigma > 1/\sigma > 1$. \square

A.1.5. Proof for Proposition 3

Proof. From (13), the gradient for a general model with slope s is:

$$\nabla_w \ell = -y \varphi(-yz) \cdot s \cdot x^*. \quad (22)$$

Taking the squared norm:

$$\|\nabla_w \ell\|_2^2 = [\varphi(-yz)]^2 \cdot s^2 \cdot \|x^*\|_2^2. \quad (23)$$

The ratio between BN and no-BN models is:

$$\begin{aligned} \frac{I_{\text{BN}}}{I_{\text{noBN}}} &= \frac{[\varphi(-yz_{\text{BN}})]^2 \cdot (a\gamma/\sigma)^2 \cdot \|x^*\|_2^2}{[\varphi(-yz_{\text{noBN}})]^2 \cdot a^2 \cdot \|x^*\|_2^2} \\ &= \frac{[\varphi(-yz_{\text{BN}})]^2}{[\varphi(-yz_{\text{noBN}})]^2} \cdot \left(\frac{\gamma}{\sigma}\right)^2. \end{aligned} \quad (24)$$

\square

A.2. Theoretical Analysis for Memorization Acceleration

Multi-Step Memorization Speedup. The per-step result in Proposition 1 raises the question of whether the single-step advantage compounds over training. We now show that it does: BN reduces the *total number of steps* required to memorize an outlier by a factor of $(\sigma/\gamma)^2$.

A.2.1. Discrete Margin Dynamics

Consider the trajectory of the margin $m_t = yz_t$ on a fixed outlier sample (x^*, y) under repeated gradient steps. From Proposition 1, the discrete dynamics are:

$$m_{t+1} = m_t + \eta \varphi(-m_t) \cdot s^2 \cdot \|x^*\|_2^2, \quad (25)$$

where $s \in \{s_{\text{noBN}}, s_{\text{BN}}\}$.

To isolate the effect of BN, define the *effective step-size* $c := \eta s^2 \|x^*\|_2^2 > 0$, so the dynamics become:

$$m_{t+1} = m_t + c \varphi(-m_t), \quad c_{\text{BN}} = \left(\frac{\gamma}{\sigma}\right)^2 c_{\text{noBN}}. \quad (26)$$

Lemma A.1 (Monotone convergence). *For any $c > 0$ and initial margin m_0 , the sequence $\{m_t\}$ defined by (26) is strictly increasing and converges to $+\infty$ as $t \rightarrow \infty$. Moreover, $\varphi(-m_t) > 0$ for all finite t , so the margin never stalls at a finite value.*

Proof. Since $\varphi(-m_t) = 1/(1 + e^{m_t}) > 0$ for all finite m_t , we have $\Delta m_t = c\varphi(-m_t) > 0$, so $m_{t+1} > m_t$ for all t . The sequence is bounded below by m_0 and strictly increasing.

To show $m_t \rightarrow \infty$: suppose for contradiction that $m_t \rightarrow M < \infty$. Then $\varphi(-m_t) \rightarrow \varphi(-M) > 0$, so $\Delta m_t \rightarrow c\varphi(-M) > 0$, contradicting convergence to a finite limit. \square

A.2.2. Continuous-Time Approximation and Time-to-Memorize

For a sharper analysis, we pass to the continuous-time limit. When c is small relative to the margin scale, the discrete dynamics (26) are well-approximated by the ODE:

$$\frac{dm}{dt} = c\varphi(-m) = \frac{c}{1 + e^m}. \quad (27)$$

This is a separable ODE whose solution we compute explicitly.

Proposition A.2 (Time-to-memorize). *Let $T(c; m_0, M)$ denote the time for the margin to travel from m_0 to a target margin $M > m_0$ under dynamics (27). Then:*

$$T(c; m_0, M) = \frac{1}{c} \left[(M + e^M) - (m_0 + e^{m_0}) \right]. \quad (28)$$

In particular, T is inversely proportional to c , and the ratio of memorization times satisfies:

$$\frac{T_{\text{noBN}}}{T_{\text{BN}}} = \frac{c_{\text{BN}}}{c_{\text{noBN}}} = \left(\frac{\gamma}{\sigma} \right)^2. \quad (29)$$

Proof. Separating variables in the ODE (27):

$$(1 + e^m) dm = c dt. \quad (30)$$

Integrating both sides from $(m_0, 0)$ to (M, T) :

$$\int_{m_0}^M (1 + e^m) dm = \int_0^T c dt = cT. \quad (31)$$

The left-hand side evaluates to:

$$\begin{aligned} \int_{m_0}^M (1 + e^m) dm &= \left[m + e^m \right]_{m_0}^M \\ &= (M + e^M) - (m_0 + e^{m_0}). \end{aligned} \quad (32)$$

Solving for T yields (28). Since the integrated quantity depends only on m_0 and M (not on c or s), the ratio $T_{\text{noBN}}/T_{\text{BN}} = c_{\text{BN}}/c_{\text{noBN}} = (a\gamma/\sigma)^2/a^2 = (\gamma/\sigma)^2$. \square

Interpretation. Theorem A.2 provides a precise prediction: BN reduces the number of training steps required to memorize an outlier to any given confidence level by a factor of exactly $(\sigma/\gamma)^2$.

For example, if $\gamma/\sigma = 5$ (consistent with early layers in our CIFAR experiments, Figure 7), BN memorizes the outlier $25\times$ faster than the no-BN baseline. This directly predicts the rapid loss convergence on noisy samples observed in Figure 2.

Remark 2 (Robustness of the scaling). The $(\gamma/\sigma)^2$ speedup in (29) holds for any target margin $M > m_0$, whether the model is in the pre-saturation regime ($m \ll 0$), near the decision boundary ($m \approx 0$), or confidently memorized ($m \gg 0$). The speedup is independent of the initial margin, the input norm, and the learning rate; it depends solely on the BN ratio γ/σ .

A.2.3. Asymptotic Regime Analysis

We further characterize the memorization dynamics in two informative regimes:

Pre-saturation regime ($m \ll 0$, early training). Here $\varphi(-m) \approx 1$, so $dm/dt \approx c$ and the margin grows approximately linearly: $m_t \approx m_0 + ct$. The BN model’s margin grows at rate $c_{\text{BN}} = (\gamma/\sigma)^2 c_{\text{noBN}}$, a $(\gamma/\sigma)^2$ speedup in this regime.

Post-saturation regime ($m \gg 0$, late training). Here $\varphi(-m) \approx e^{-m}$, so:

$$\frac{dm}{dt} \approx c e^{-m} \implies m(t) \approx \log(ct + e^{m_0}). \quad (33)$$

The margin grows logarithmically. The BN model still maintains its advantage: at the same wall-clock step t , $m_{\text{BN}}(t) - m_{\text{noBN}}(t) \approx 2\log(\gamma/\sigma)$.

This two-regime behavior matches our empirical observations: early in training, BN models show dramatically faster loss reduction on noisy samples (Figure 2); later, both models converge but BN models reach lower loss values, consistent with the persistent logarithmic advantage.

A.3. Theoretical Discussion and Limitations

Why outliers are disproportionately affected. Although our analysis applies to any sample, outliers experience stronger amplification through three compounding mechanisms:

1. *Persistent tail activations.* Outliers maintain large $|h - \mu|$ throughout training, placing them in tail regions where BN’s rescaling has maximal effect. Typical samples cluster near μ where the rescaling is minimal.
2. *Channel specialization.* Channels with small σ correspond to specialized features with low activation variance across typical data. Outliers, by definition, activate features atypically, and these low- σ channels produce

Algorithm 1: Corrupted label data synthesis

Input : Dataset D , classes set C , flipping ratio k **Output:** Set D' that contains label flipping instancesInitialize $D' = \emptyset$; $\delta = |D| \cdot k$;**while** $|D'| < \delta$ **do**

┌	randomly pick $(x, y) \in D$;
├	randomly pick $y^* \in C/\{y\}$;
├	$D' = D'.\text{insert}(\{(x, y^*)\})$;
└	$D = D/\{(x, y)\}$;

 $D' = D'.\text{union}(D)$;**return** D' ;

the largest γ/σ ratios. Our layerwise analysis (Figure 7) confirms that early layers—which capture lower-level features with higher specialization—exhibit the largest γ/σ values.

3. *Self-reinforcing dynamics.* As shown in Theorem 1, outliers disproportionately drive γ growth, which further amplifies their own memorization. This feedback loop is absent in no-BN models.

Multi-layer amplification. In an L -layer network, each BN layer l applies its own rescaling with ratio γ_l/σ_l . During backpropagation, the gradient at the input layer accumulates contributions from all BN layers. While the exact interaction is complex and depends on network architecture, the effective amplification involves terms of the form $\prod_{l=1}^L (\gamma_l/\sigma_l)$. Our empirical observation that γ/σ is highest in early layers (Figure 7) suggests that the total amplification can be substantially larger than what a single-layer analysis predicts.

Implications for differential privacy. The amplified gradient norm under BN has direct consequences for differentially private training. In DP-SGD, per-sample gradients are clipped to a threshold C before aggregation and noise addition. Since BN amplifies outlier gradient norms by $(\gamma/\sigma)^2$, either: (a) the clipping threshold must be set higher (increasing the noise needed for the same privacy guarantee), or (b) more information about outliers is lost to clipping (biasing the model away from memorizing them). This suggests a formal tension between BN and differential privacy that merits further investigation.

Limitations. Our theoretical analysis relies on several simplifications:

1. *Single-layer architecture.* Real networks are deep and involve complex interactions between BN layers. However, our single-layer result captures the local per-channel mechanism, and the multi-step analysis (Theorem A.2) shows this compounds over training.
2. *Fixed batch statistics.* We treat (μ, σ) as fixed within

Algorithm 2: OOD data synthesis

Input : Dataset D , other dataset D^* , label class C , noisy data ratio k **Output:** Set D' that contains noisy instancesrandomly pick a specific label $y \in C$;randomly select $X^* = \{x : (x, \cdot) \in D^*\}$; $\delta = |D| \cdot k$;initialize $D' = \emptyset$;initialize $i = 0$;**while** $i < \delta$ **do**

┌	randomly pick $x \in X^*$;
├	$D' = D'.\text{insert}(\{(x, y)\})$;
└	$i \leftarrow i + 1$;

 $D' = D'.\text{union}(D)$;**return** D' ;

each step. In practice, batch composition varies, and outlier presence affects μ and σ . When an outlier is *in* the mini-batch, it slightly shifts μ and inflates σ , partially moderating the amplification for that specific step. However, the outlier appears in only $1/B$ of mini-batches (for batch size B), so the amplification operates at full strength for the remaining $(B - 1)/B$ fraction of steps.

3. *Independent γ and σ dynamics.* In reality, changes to w affect both the activation distribution (and hence σ) and the loss landscape. Our analysis treats these as decoupled over short time horizons.

Despite these simplifications, the core prediction— $(\gamma/\sigma)^2$ amplification that compounds over training—is validated by our experiments showing (a) amplified gradient norms (Figure 4), (b) faster convergence on noisy data (Figure 2), (c) $\gamma/\sigma > 1$ across layers and datasets (Figure 7), and (d) increased vulnerability to membership inference (Figures 5–6).

B. Corrupted data synthesis pseudos

We perform data synthesis using two strategies to create a corrupted label dataset and an out-of-distribution dataset. Details of these algorithms are shown in Algorithm 1 and Algorithm 2.

C. Detailed experiments analysis

C.1. Extended analysis of γ/σ ratios

Figure 9 shows the ratio between the scale γ and the variance parameters σ of BN in Lenet, training across multiple datasets and multiple noisy factor k . Over multiple settings, the results consistently confirm that the ratio γ/σ is much greater than 1 on all model layers. Connected with Proposition 3, the ratio highlights the strong gradient norm amplification on corrupted samples, therefore increasing the model

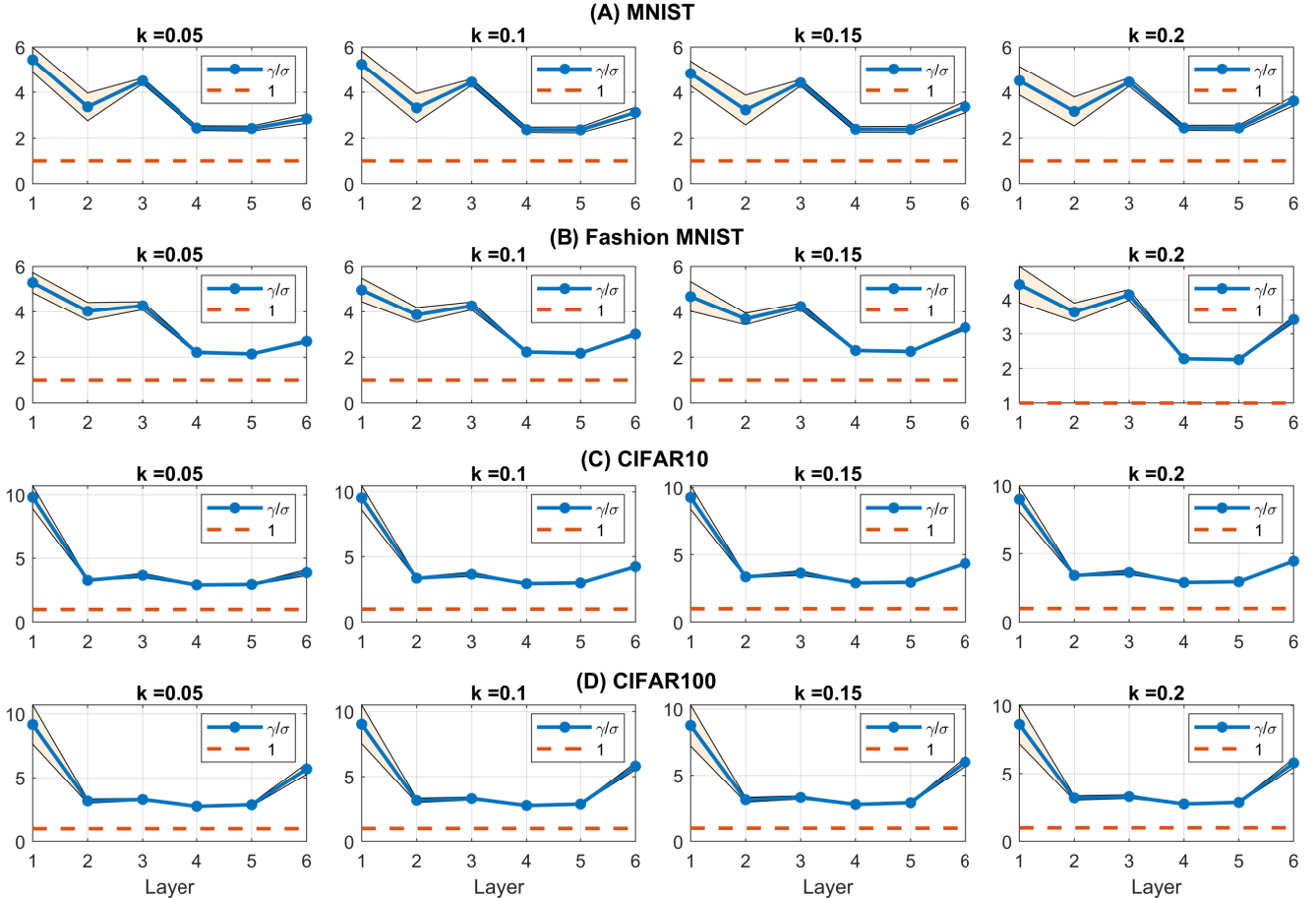


Figure 9. Ratio between two parameters (γ , σ) of Batch Norm layers of Lenet training on datasets with $k = 0.1$. (Median values of repeated five running times)

memorization of these data points.

C.2. Learning characteristics analysis

Figure 10 presents training loss curves on CIFAR10 of Lenet, Resnet34, Resnet50 over various values of $k \in \{5\%, 10\%, 15\%, 20\%, 25\%, 30\%\}$. There are four curves for each sub-figure including the accuracy of models with and without BN on a clean set (nonmem-set) and a noisy set (mem-set). Since the trends of models with BN decrease dramatically and below the curves of models without BN, it highlights the fast convergence speed and memorization for models incorporating BN on both clean and noisy set.

C.3. Extended analysis of memorization on OOD data

Figure 11 shows the memorization capacity of BN model and the no-BN model in OOD data distribution with respect to various values $k \in \{0.05, 0.1, 0.15, 0.2, 0.25, 0.3\}$ with different model architectures. Generally, our observation is consistent among OOD ratios, where the performance of

models incorporating BN is higher than ones without BN by more than 3%. It indicates that BN increases the memorization effects on the OOD set.

C.4. MIA on baseline datasets (without OOD)

Algorithm description. Along with the study of the privacy attack on OOD datasets, we further explore the sensitivity of models integrating BN solely on clean datasets. Intuitively, this setting encourages the MIA algorithm to concentrate on samples that are naturally memorized by the model’s viewpoint rather than manually created noisy samples by data viewpoints. Specifically, ResNet-based architectures are trained on the clean CIFAR-10 dataset. After that, we exploit the LIRA attack and measure the success rate by AUC metrics to compare the vulnerable leakage between BN models and no-BN models.

Results. Our results in Figure 12 illustrate that even in the clean setting, models including BN achieve higher attacking AUC at least 1% than models excluding BN. This result

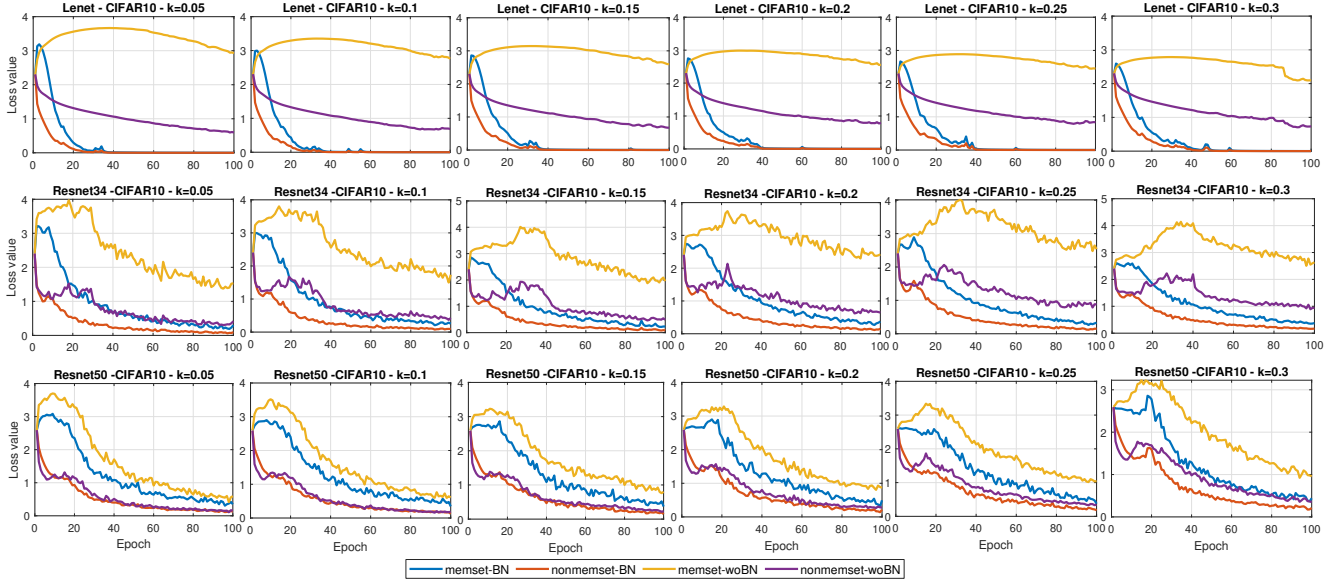


Figure 10. Loss values (a mean of five times repeating) by epoch on a memset (the original data) and a nonmemset (the flipped data) of models using BN and without using BN.

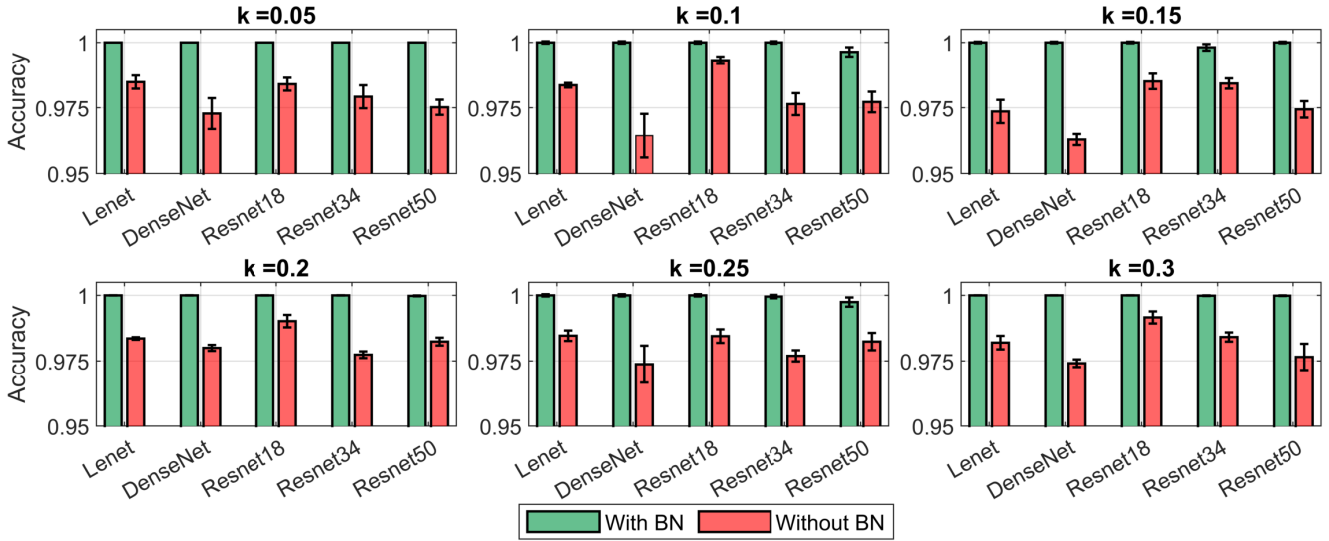


Figure 11. Comparison of memorization performance of model training with and without BN on natural OOD data across different neural architectures.

indicates that models incorporating BN are more privacy vulnerable against MIA than models with no BN.

C.5. MIA results statistical comparison

Fig. 14 shows that the variance in MIA across architectures and ratios is similar between BN and no-BN. A one-tailed t-test evaluating whether MIA is less effective on BN models yields a p-value of 0.11% ($< 5\%$), rejecting this hypothesis.

D. Experimental setup details

Hyperparameters. We train all models for 200 epochs on the respective classification datasets. Adam optimizer is used with the fixed learning rate equal to $1e^{-4}$ and batch size 256. We disable data augmentation and dropout layers to mitigate the randomness during training. To ensure the robustness of our results, each experiment is repeated five times, and we report the mean and standard deviation of the obtained performance metrics.

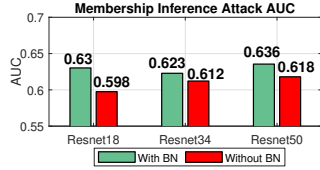


Figure 12. Comparison of memorization performance of model training with and without BN on the clean dataset across different neural architectures.

MIA settings. We use 32 shadow models with architectures matching the target model to approximate its behavior. As a SOTA MIA method, LIRA motivates our choice over loss-threshold or metric-based attacks to measure privacy leakage in models with and without BN layers.

Evaluation metrics. We employ different evaluation metrics to analyse the effect under three distinct scenarios. For *noisy data influence*, we use classification accuracy to quantify the degree of memorization of models on noisy datasets. For *membership inference attack influence* setting, the Receiver Operating Characteristics (ROC) curve and Area Under the Curve (AUC) is used to evaluate the memorization effects under adversarial setting. Finally, we adopt sample-wise gradient metrics for *per-sample influence* setting, which quantify the influence of each sample on the learned model.

E. Ablation studies

E.1. Effect of learning rates

In order to assess the behavior of models incorporating BN on a memorization setting, we conduct an experiment of BN effect on memorization with $lr = 1e^{-3}$, which is shown in Figure 13. Diverged models are exploited, such as Lenet (A), Densenet (B), Resnet18 (C), Resnet34 (D), and Resnet50 (E) with varied corrupted labels ratio $k \in \{5\%, 10\%, 15\%, 20\%, 25\%, 30\%\}$. The observation is still similar to our finding in the main paper. The no-BN models show a low performance on noisy data (18/20 cases), hence indicating a weak memorization capacity compared to models with BN layers.

E.2. Effect of batch sizes

We study the effect of batch size in the forced memorization setting (Fig 15). The results confirm increased memorization in BN models across batch sizes.

E.3. Effect of optimizers

Figure 16 confirms that models with BN (green, yellow lines) have a stronger memorization accuracy than models without BN (red, purple lines).

E.4. Effect of normalization techniques

We analyze memorization capacity of ResNet18/34 with GroupNorm (GN), InstanceNorm (IN), LayerNorm (LN), and BatchNorm (BN) on CIFAR-10. Figure 17 shows **all normalization strategies consistently amplify memorization** compared to no normalization across all corruption ratios k .

E.5. Effect of model architectures

Algorithm description. In this section, we additionally study the privacy vulnerability of the Layer Normalization (LN) layer, which has been widely used on transformer-based architectures—the backbone of recent foundation models. The key advantage of LN compared to BN is that it is independent on the mini-batch size and consistent between training and testing times, hence stabilizing the training procedures, especially on the sequential models. In particular, LN computes mean and standard variation statistics through individual neurons in the layer rather than through samples of a mini-batch like BN. To analyze the impact of LN on privacy, we adopt Vision Transformer (ViT) with the inclusion and removal of LN and train on the corrupted labels dataset.

Results. Table 1 presents accuracy of ViT with and without LN on corrupted label datasets with the noisy ratio $k \in \{0.01, 0.05\}$. The result shows that ViT with LN is dominated in accuracy compares to the one without LN. Models incorporating LN can fit very well on the out-of-distribution data, hence demonstrating the capacity of memorization depended on LN layers.

E.6. Effect of complex dataset

We report the performance of ResNet34 on two complex datasets: SVHN and TinyImageNet (c.f. Fig 19). These results are consistent with our observation that BN increases memorization.

F. Trade-off between memorization and generalization

Figure 18 shows test accuracy alongside memorization accuracy. The gap in test accuracy is smaller than the memorization gap, indicating that removing BN sacrifices modest generalization while substantially reducing privacy risk. Moreover, Fig. 20 unifies 3 aspects, comparing BN and no-BN. Increased memorization accuracy corresponds to higher privacy vulnerability under MIA but higher accuracy on the clean dataset.

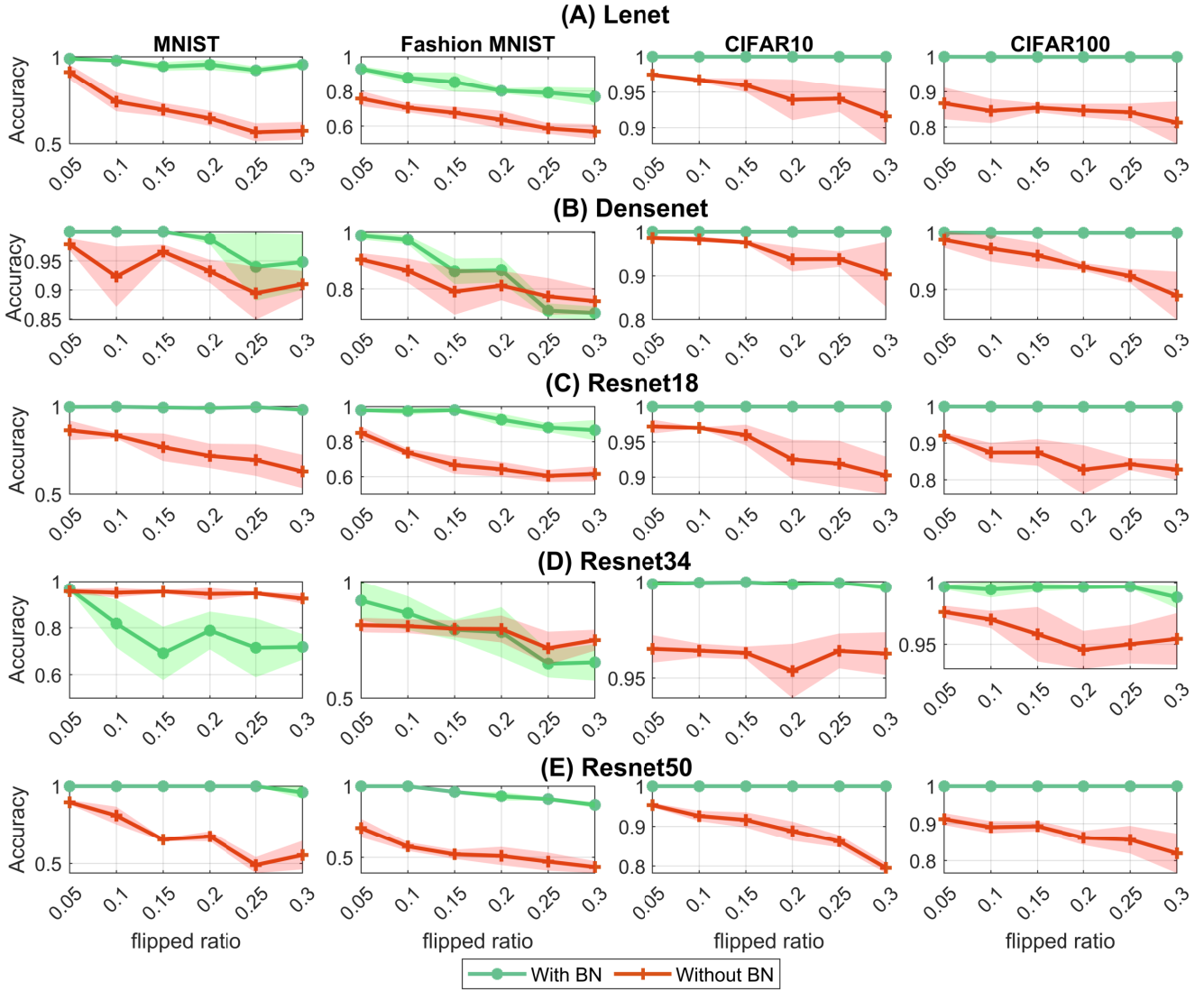


Figure 13. Accuracy of Lenet, DenseNet, Resnet18, Resnet34 with and without BN on noisy set of MNIST, FashionMNIST, CIFAR10 and CIFAR100 using 10^{-3} learning rate (Best view in color)

Method	MNIST	FashionMNIST	CIFAR10	CIFAR100
ViT ($k = 1\%$)	0.993±0.001	0.993±0.003	0.997±0.002	1.0±0.0
ViT w/o LN ($k = 1\%$)	0.055±0.006	0.055±0.01	0.259±0.037	0.494±0.11
ViT ($k = 5\%$)	0.992±0.001	0.995±0.003	0.999±0.002	0.999±0.0
ViT w/o LN ($k = 5\%$)	0.135±0.065	0.157±0.098	0.212±0.033	0.466±0.243

Table 1. Performance of ViT with the inclusion and removal of Layer Norm on the corrupted labels dataset.

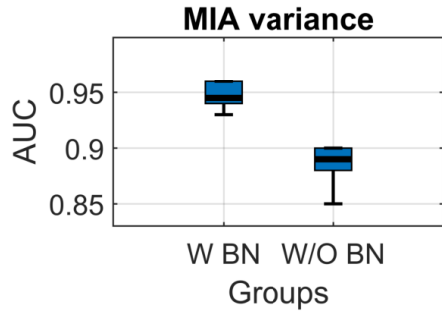


Figure 14. MIA Variance

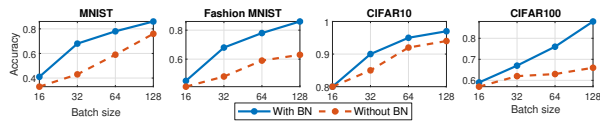


Figure 15. Batch size comparison on ResNet18 (5%).

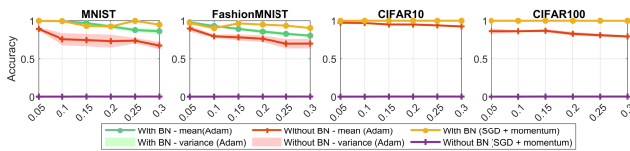


Figure 16. Performance of ResNet18 with different optimizers

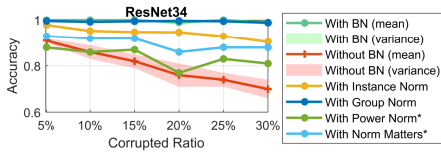


Figure 17. Performance of models with different normalization techniques over multiple corrupted ratios

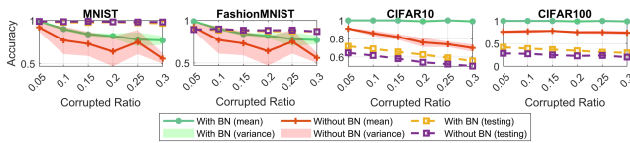


Figure 18. Performance of ResNet34 on various datasets (Best view in color)

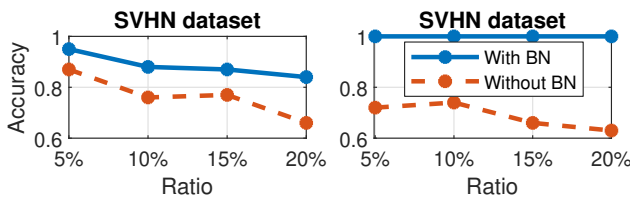


Figure 19. Memorization accuracy in SVHN and Tiny ImageNet

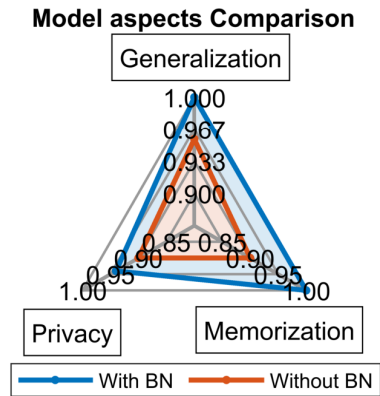


Figure 20. ResNet34 Gen, Mem and MIA